

# Target Handover in Distributed Integrated Sensing and Communication

Yu Ge<sup>\*</sup>, Ossi Kaltiokallio<sup>†</sup>, Hui Chen<sup>\*</sup>, Jukka Talvitie<sup>†</sup>, Yuxuan Xia<sup>‡</sup>, Giyyarpuram Madhusudan<sup>§</sup>,  
Guillaume Larue<sup>§</sup>, Lennart Svensson<sup>\*</sup>, Mikko Valkama<sup>†</sup>, Henk Wymeersch<sup>\*</sup>

<sup>\*</sup>Department of Electrical Engineering, Chalmers University of Technology, Gothenburg, Sweden,

<sup>†</sup>Unit of Electrical Engineering, Tampere University, Tampere, Finland,

<sup>‡</sup>Department of Automation, Shanghai Jiaotong University, Shanghai, China, <sup>§</sup>Orange Research, Meylan, France

**Abstract**—The concept of 6G distributed integrated sensing and communications (DISAC) builds upon the functionality of integrated sensing and communications (ISAC) by integrating distributed architectures, significantly enhancing both sensing and communication coverage and performance. In 6G DISAC systems, tracking target trajectories requires base stations (BSs) to hand over their tracked targets to neighboring BSs. Determining what information to share, where, how, and when is critical to effective handover. This paper addresses the target handover challenge in DISAC systems and introduces a method enabling BSs to share essential target trajectory information at appropriate time steps, facilitating seamless handovers to other BSs. The target tracking problem is tackled using the standard trajectory Poisson multi-Bernoulli mixture (TPMBM) filter, enhanced with the proposed handover algorithm. Simulation results confirm the effectiveness of the implemented tracking solution.

**Index Terms**—6G, DISAC, tracking, trajectory, target handover, TPMBM.

## I. INTRODUCTION

Integrated sensing and communications (ISAC) has attracted attention in the advancement of 5G mobile radio systems and is expected to play a pivotal role in shaping 6G networks [1], [2]. However, the current ISAC framework often overlooks critical aspects, such as enabling large-scale deployments that can monitor numerous connected user devices and passive objects over wide areas and extended periods [3]–[5]. To address these limitations, the concept of distributed integrated sensing and communications (DISAC) has emerged, which expands ISAC functionality through distributed architectures, enhancing its capabilities in decentralized systems. In addition, DISAC is set to revolutionize various sectors, including transportation, and automation [3], [4].

In a monostatic DISAC system, several base stations (BSs) transmit orthogonal signals that bounce off the environment and are received by the same BS, ensuring full knowledge of both the transmitted signals and the clock [6], [7]. Due to the limited transmission power and hardware limitations, each BS can only track targets within its field-of-view (FoV). As a result, without information sharing between BSs, each BS can only track target trajectories for a limited time and only within its own FoV. To enable more comprehensive

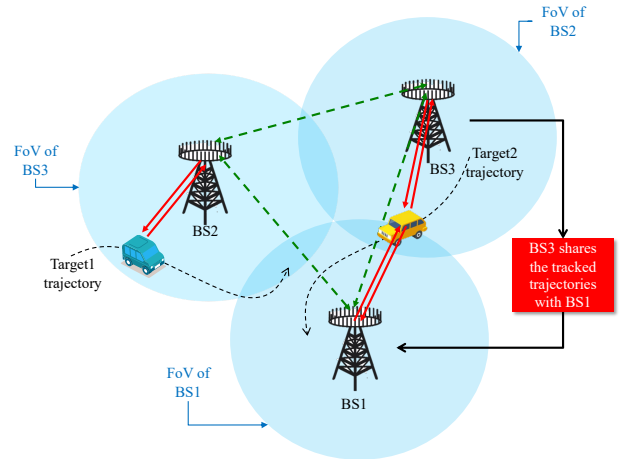


Fig. 1. An example of the target handover problem in a monostatic DISAC system. Targets move over time, and each BS can only observe those within its own FoV. Each BS independently processes its local observations to track the targets, then shares the tracked trajectories with neighboring BSs (i.e., with overlapping or adjacent FoV).

tracking without extensive data sharing, BSs must *hand over targets* to neighboring BSs when necessary. This allows the continuation of target trajectories across BSs while minimizing communication between them. This setup is depicted in Fig. 1. Deciding what information to share, as well as when, where, and how to share it, is crucial for efficient handover.

Related works can be categorized into those addressing the multi-target tracking (MTT) sensing problem systems and those focusing on target handover between different BSs or sensors. The sensing challenge has been explored extensively and explored through various methods in the MTT literature [7]–[11]. Among these, random finite set (RFS)-based methods [7], [10], [11] can effectively manage key challenges such as unknown data associations (DAs), an uncertain number of targets, unknown target states, missed detections, and false alarms, and can also generate entire target trajectories without increasing the computational complexity [12], [13]. However, these methods either rely on data from a single source or use a fusion center to combine sensing results from multiple sources, without incorporating any target handover mechanism. The concept of *target handover* has been addressed in various forms [14]–[16], primarily in the context of networked radar systems. In [14] a binary linear

This work has been supported by the SNS JU project 6G-DISAC under the EU's Horizon Europe research and innovation Program under Grant Agreement No 101139130.

programming approach is used to schedule radars in order to maximize the tracking duration of targets. In [15], the concept of handover refers to the association between moving sensors and static coordinators, and is thus similar to *user equipment (UE) handover* in communication systems [16], [17]. Hence, the problem of target handover remains largely unexplored.

In this paper, we explore the target handover problem in the DISAC system, enabling each BS to track complete target trajectories within its FoV from origin until they exit the FoV, by sharing necessary trajectory information among BSs. The main contributions of this paper are as follows: (i) We propose an RFS-based target handover algorithm that facilitates trajectory sharing between neighboring BSs, ensuring smooth trajectory tracking as the targets enter their FoVs, along with detailed execution steps; (ii) We extend the standard trajectory Poisson multi-Bernoulli mixture (TPMBM) filter at each BS by incorporating the proposed target handover mechanism; (iii) We validate the effectiveness of the proposed target handover mechanism through simulations in a mmWave radio network, demonstrating that it allows BSs to track targets' trajectories from their origin, while also enhancing sensing performance when targets transition into new FoVs.

*Notations:* Scalars (e.g.,  $x$ ) are denoted in italic, vectors (e.g.,  $\mathbf{x}$ ) in bold lower-case letters, matrices (e.g.,  $\mathbf{X}$ ) in bold capital letters, sets (e.g.,  $\mathcal{X}$ ) in calligraphic. Transpose is denoted by  $(\cdot)^\top$ , the Hermitian transpose is denoted by  $(\cdot)^H$ , the union of mutually disjoint sets is denoted by  $\cup$ , a Gaussian density with mean  $\mathbf{u}$  and covariance  $\Sigma$ , evaluated in value  $\mathbf{x}$ , is denoted by  $\mathcal{N}(\mathbf{x}; \mathbf{u}, \Sigma)$ , and  $d_x = \dim(\mathbf{x})$ .

## II. SYSTEM MODEL

We consider a scenario with multiple BSs and multiple targets, as depicted in Fig. 1. Each BS has limited FoV, and can only see the targets in its FoV. The FoVs of two neighboring BSs can overlap. Each individual BS performs monostatic sensing to track the moving targets in its FoV, and it can share the information on target tracks to nearby BSs. In this section, the state models, the received signal model, and the measurement model are introduced.

### A. State Models

Each BS is deployed with a uniform rectangular array (URA). The state of the  $p$ -th BS contains a 3D location  $\mathbf{s}_{\text{BS}}^p$ , representing the position of the center of the URA, and its 3D orientation  $\psi_{\text{BS}}^p$ . The number of BSs and all BS states are known. While multiple targets in the considered environment are moving over time, neither the number of targets nor the target states are known to the BSs. We denote  $\mathbf{x}_k^i = [(\mathbf{s}_k^i)^\top, (\dot{\mathbf{s}}_k^i)^\top]^\top$  as the dynamic state of the  $i$ -th target at time step  $k$ , containing its 3D position  $\mathbf{s}_k^i$  and its 3D velocity  $\dot{\mathbf{s}}_k^i$ . We assume the transition density of each target can be described by

$$f(\mathbf{x}_{k+1}^i | \mathbf{x}_k^i) = \mathcal{N}(\mathbf{x}_{k+1}^i; \mathbf{v}(\mathbf{x}_k^i), \mathbf{Q}_{k+1}), \quad (1)$$

where  $\mathbf{v}(\cdot)$  represents the known transition function and  $\mathbf{Q}_{k+1}$  is the known process noise covariance.

### B. Signal Models

Every time step, each BS sends out downlink orthogonal frequency-division multiplexing (OFDM) pilot signals, which are altered by the objects in the environment and then possibly received by the BS. At the  $p$ -th BS side, the received signal at the subcarrier  $\kappa$  and the time step  $k$  can be described as [18]

$$\mathbf{Y}_{\kappa,k}^p = \mathbf{H}_{\kappa,k}^p \mathbf{S}_{\kappa,k}^p + \mathbf{N}_{\kappa,k}^p, \quad (2)$$

with  $\mathbf{S}_{\kappa,k}^p$  denoting the potentially pre-coded pilot signal over subcarrier  $\kappa$ ,  $\mathbf{Y}_{\kappa,k}^p$  denoting the received signal over subcarrier  $\kappa$ ,  $\mathbf{N}_{\kappa,k}^p$  denoting the additive white Gaussian noise, and  $\mathbf{H}_{\kappa,k}^p$  being the channel frequency response. The transmitted signals may be bounced back to the  $p$ -th BS from multiple targets, and we assume that  $\mathbf{H}_{\kappa,k}^p$  can be expressed as

$$\mathbf{H}_{\kappa,k}^p = (\mathbf{W}_k^p)^H \sum_{i=1}^{I_k^p} g_k^{p,i} \mathbf{a}_{\text{BS}}^p(\boldsymbol{\theta}_k^{p,i}) (\mathbf{a}_{\text{BS}}^p(\boldsymbol{\theta}_k^{p,i}))^H e^{-j2\pi\kappa\Delta f\tau_k^{p,i}},$$

where  $\mathbf{W}_k^p$  represents a combining matrix at the  $p$ -th BS side,  $\mathbf{a}_{\text{BS}}^p(\cdot)$  denotes the steering vector of the antenna array of the  $p$ -th BS, and  $\Delta f$  denotes the subcarrier spacing. There are  $I_k^p$  visible objects in the FoV of the  $p$ -th BS, which can bounce signals back to the corresponding BS and generates  $I_k^p$  paths by assuming a point object model. Each path can be described as a complex gain  $g_k^{p,i}$ , a time of arrival (TOA)  $\tau_k^{p,i}$ , and an angles of arrival (AOA) pair  $\boldsymbol{\theta}_k^{p,i}$  in both azimuth and elevation. As the BS can only receive bounced signals, there is no line-of-sight (LOS) path, and the BS is always synchronized with itself, so there is no clock bias issue, resulting in  $\tau_k^{p,i} = 2\|\mathbf{s}_{\text{BS}}^p - \mathbf{s}_k^i\|/c$  for a target with 3D position  $\mathbf{s}_k^i$ , where  $c$  denotes the speed of light. Moreover, we assume only single-bounce paths exist, therefore, the AOA is equal to the corresponding angles of departure (AOD). The relations between AOA/AOD and the geometric state can be found in [19, Sec. 2.2]. Note that Doppler effects are not considered due to the short transmission interval. However, incorporating Doppler measurements would significantly enhance the detection and tracking performance of the mobile targets.

### C. Measurement Models

At each BS side, a channel estimator [20]–[22] is applied on the received signals  $\mathbf{Y}_{\kappa,k}^p$  in (2) to obtain the estimates of channel parameters of TOA and AOA, given the information on the sent signals  $\mathbf{S}_{\kappa,k}^p$  and the combining matrix  $\mathbf{W}_k^p$ . To focus this work, we assume the channel parameter estimates are directly available to be used as measurements for sensing purposes. We model the measurements provided by the channel estimator at the  $p$ -th BS and the time step  $k$  as a RFS, i.e.,  $\mathcal{Z}_k^p = \{\mathbf{z}_k^{p,1}, \dots, \mathbf{z}_k^{p,\hat{I}_k^p}\}$ , with  $\hat{I}_k^p$  denoting the number of resolved paths. Note that usually  $\hat{I}_k^p \neq I_k^p$ , as there could be also some clutter measurements originated from noise peaks during channel estimation, and not all paths can be resolved resulting in misdetections of some targets. These clutter measurements are modeled as a Poisson point process (PPP), parameterized by the intensity function  $c(\mathbf{z})$ . Since targets may also be undetected, we introduce the detection probability  $p_D(\mathbf{s}_{\text{BS}}^p, \mathbf{s}_k^i) \in [0, 1]$  to capture the possibility of obtaining a measurement from an object located at  $\mathbf{s}_k^i$ , detected

by the  $p$ -th BS. Assuming that the measurement  $\mathbf{z}^{p,i}$  originates from the object located at  $\mathbf{s}^i$ , its likelihood is modeled as

$$f(\mathbf{z}_k^{p,i} | \mathbf{s}_{\text{BS}}^p, \mathbf{s}_k^i) = \mathcal{N}(\mathbf{z}_k^{p,i}, \mathbf{h}(\mathbf{s}_{\text{BS}}^p, \mathbf{s}_k^i), \mathbf{R}_k^{p,i}), \quad (3)$$

where  $\mathbf{h}(\mathbf{s}_{\text{BS}}^p, \mathbf{s}_k^i) = [\tau_k^{p,i}, (\boldsymbol{\theta}_k^{p,i})^\top]^\top$  represents the nonlinear function that transforms the geometric information to TOA and AOA [19, Sec. 2.2], and  $\mathbf{R}_k^{p,i}$  denotes the known associated measurement covariance. However, it is important to note that the DA remains unknown, making it unclear which source each measurement originates from.

### III. DECENTRALIZED MTT PER BS

In this section, we describe how each BS tracks targets within its FoV over time using a TPMBM filter [23], which estimates a set of target trajectories rather than a set of individual target states, enabling trajectory estimation without increasing the computational complexity. We will introduce the trajectory state representation and the high-level operation of the TPMBM filter. For additional details on the the TPMBM density, we refer to the Appendix. For notational brevity, we drop the BS index  $p$  throughout this section.

#### A. Trajectory State Representation

As described in Section II-A, a single target state contains essential information about the target, such as its 3D position and 3D velocity. However, our objective is to track targets over time, aiming to estimate target trajectories rather than individual target states at specific time steps. A target trajectory is a finite sequence of target states, starting at any time step and ending at a later one. The trajectory state of a target can be modeled as a tuple [12], [13]  $\mathbf{X} = (\mu, \nu, \mathbf{x}_{\mu:\nu})$ , where  $\mu$  denotes the birth time step of the trajectory, i.e., the time step when the trajectory begins,  $\nu$  indicates the time step of the trajectory's most recent state, i.e., the time step when it ends, and  $\mathbf{x}_{\mu:\nu}$  denotes the sequence of target states from the time step  $\mu$  to the time step  $\nu$ , i.e.,  $\mathbf{x}_\mu, \dots, \mathbf{x}_\nu$ . If the current time step is  $k$ , then  $\nu = k$  represents the trajectory is still ongoing, whereas  $\nu < k$  signifies that the trajectory ended at time step  $\nu$ . The trajectory cannot end before it begins so that  $\mu \leq \nu$ , and  $(\nu - \mu + 1)$  represents the length of the trajectory. Similar to a set of targets, we can model a set of trajectory as a RFS  $\mathcal{X} = \{\mathbf{X}^1, \dots, \mathbf{X}^{|\mathcal{X}|}\}$ , modeled as a TPMBM RFS.

#### B. TPMBM Filter

Each BS needs to track the trajectories of all targets  $\mathcal{X}_k$  within its FoV over time, using the received measurements  $\mathcal{Z}_k$  (as introduced in Section II-C) as input every time step. This can be accomplished by implementing a TPMBM filter [23], [24] on each BS. The primary objective of the TPMBM filter is to recursively compute the posterior  $f(\mathcal{X}_k | \mathcal{Z}_k)$  at each time step, following the prediction and update steps of the Bayesian filtering framework for trajectory RFSs [23]

$$f(\mathcal{X}_{k+1} | \mathcal{Z}_{1:k}) = \int f(\mathcal{X}_k | \mathcal{Z}_{1:k}) f(\mathcal{X}_{k+1} | \mathcal{X}_k) \delta \mathcal{X}_k, \quad (4)$$

$$f(\mathcal{X}_{k+1} | \mathcal{Z}_{1:k+1}) = \frac{f(\mathcal{X}_{k+1} | \mathcal{Z}_{1:k+1}) \ell(\mathcal{Z}_{k+1} | \mathcal{X}_{k+1})}{\int f(\mathcal{X}_{k+1} | \mathcal{Z}_{1:k}) \ell(\mathcal{Z}_{k+1} | \mathcal{X}_{k+1}) \delta \mathcal{X}_{k+1}}, \quad (5)$$

where  $f(\mathcal{X}_{k+1} | \mathcal{X}_k)$  denotes the transition density of the trajectory set,  $\ell(\mathcal{Z}_{k+1} | \mathcal{X}_{k+1})$  denotes the RFS likelihood function of

the measurement set give the trajectory set, and  $\int \psi(\mathcal{X}) \delta \mathcal{X}$  indicates the trajectory set integral [13]. The expressions (4)–(5) effectively serve to predict and update the TPMBM components. For further details, please refer to [23], [24].

The output of the TPMBM filter after each time step  $k$  is a TPMBM density, which has the following components:  $\lambda_{k|k}(\mathbf{X})$  represents the intensity function of the undetected trajectories, while  $\{w_{k|k}^j, \{r_{k|k}^{j,i}, f_{k|k}^{j,i}(\mathbf{X})\}_{i \in \mathbb{I}_{k|k}^j}\}_{j \in \mathbb{I}_{k|k}}$  represents the state densities of the trajectories of the detected targets under different DA hypotheses. Here,  $w_{k|k}^j$  is a global hypothesis weight,  $r_{k|k}^{j,i}$  is the existence probability of the  $i$ -th target under the  $j$ -th hypothesis, and  $f_{k|k}^{j,i}(\mathbf{X})$  is the corresponding trajectory state density, which can be factorized into  $f_{k|k}^{j,i}(\mathbf{x}_{\mu:\nu} | \mu, \nu)$  and  $f_{k|k}^{j,i}(\mu, \nu)$  [24, Eq. 4]. In this paper, we focus on the Gaussian implementation of the TPMBM filter [23, Sec. V].

### IV. MTT WITH TARGET HANDOVER

Each BS locally applies a TPMBM filter to track targets within its FoV. However, since each BS has a limited FoV, and the targets move over time, some targets will inevitably exit the FoVs of some BSs and enter the FoVs of neighboring BSs. Although a BS may lose track of targets as they leave its FoVs, it can hand over these targets to the neighboring BSs to maintain continuous tracking.<sup>1</sup> This section introduces the algorithm designed for efficient target handover between BSs.

#### A. Handover Information

We assume that all BSs can communicate with each other, and each BS is aware of its own and all other BSs' FoVs. Target handover only occurs between neighboring BSs, as a target leaving one BS's FoV can only enter the FoVs of nearby BSs. To reduce communication load, a BS only shares information about tracked target trajectories with the neighboring BSs into whose FoVs those targets are expected to enter. This communication happens after the prediction step of the local TPMBM filter at each BS.

The first step is to determine if any targets are likely to move into another BS's FoV at each BS. Consider the  $m$ -th BS at time step  $k+1$ , suppose the predicted prior density  $f(\mathcal{X}_{k+1}^m | \mathcal{Z}_{1:k}^m)$  consists of the TPMBM components  $\lambda_{k+1|k}^m(\mathbf{X})$  and  $\{w_{k+1|k}^{m,j}, \{r_{k+1|k}^{m,j,i}, f_{k+1|k}^{m,j,i}(\mathbf{X})\}_{i \in \mathbb{I}_{k+1|k}^{m,j}}\}_{j \in \mathbb{I}_{k+1|k}^m}$ . The  $j, i$ -th predicted trajectory is said to be entering the FoV of the  $m'$ -th BS, if

$$r_{k+1|k}^{m,j,i} \int f_{k+1|k}^{m,j,i}(\mathbf{s}_{k+1}) p_{\text{D}}(\mathbf{s}_{k+1}, \mathbf{s}_{\text{BS}}^{m'}) d\mathbf{s}_{k+1} \geq \gamma, \quad (6)$$

where  $f_{k+1|k}^{m,j,i}(\mathbf{s}_{k+1})$  represents the predicted position density of the tracked target at the  $m$ -th BS at time step  $k+1$ , obtained during the prediction step of the TPMBM filter,  $p_{\text{D}}(\mathbf{s}_{k+1}, \mathbf{s}_{\text{BS}}^{m'})$  denotes the detection probability at the  $m'$ -th BS, and  $\gamma$  is a predetermined threshold. Second, in case (6) holds true, the  $m$ -th BS should inform the  $m'$ -th BS of the target's trajectory details, facilitating the handover of tracking responsibilities.

<sup>1</sup>We do not consider the fully centralized approach, which requires BSs to share all received measurements to a fusion center.

The trajectory information that needs to be shared includes the existence probability  $r_{k+1|k}^{m,j,i}$ , the trajectory density  $f_{k+1|k}^{m,j,i}(\mathbf{X})$ , and the global hypothesis weight  $w_{k+1|k}^{m,j}$ . To efficiently hand over this information, we approximate it using a trajectory PPP,<sup>2</sup> and the trajectory PPP intensity is formulated as follows

$$\lambda_{H,k+1|k}^{m,j,i} = w_{k+1|k}^{m,j} r_{k+1|k}^{m,j,i} f_{k+1|k}^{m,j,i}(\mathbf{X}). \quad (7)$$

This PPP intensity can be seamlessly incorporated into the predicted trajectory PPP intensity of the  $m'$ -th BS  $\lambda_{k+1|k}^{m'}(\mathbf{X})$ , and the resulting combined trajectory PPP intensity is expressed as

$$\lambda_{k+1|k}^{m'}(\mathbf{X}) \leftarrow \lambda_{k+1|k}^{m'}(\mathbf{X}) + \lambda_{H,k+1|k}^{m,j,i}(\mathbf{X}). \quad (8)$$

To minimize unnecessary handovers and corresponding inter-BS data exchange, each BS only hands over targets that have not been recently shared with the destination BS.<sup>3</sup>

### B. Target Handover Algorithm

We examine all the detected trajectories at each BS to identify any trajectories that may enter the FoVs of neighboring BSs every time step, adding the corresponding trajectory PPP intensities to the predicted trajectory PPP intensities. Meanwhile, the trajectory MBM components remain unchanged, as no modifications occur in that regard. The resulting algorithm is summarized in Algorithm 1.

#### Algorithm 1 Target Handover Algorithm

**Input:** Predicted  $\{w_{k+1|k}^{m,j}, \{r_{k+1|k}^{m,j,i}, f_{k+1|k}^{m,j,i}(\mathbf{X})\}_{i \in \mathbb{I}_{k|k}^{m,j}}\}_{j \in \mathbb{I}_{k|k}^m}$ ,

$$\lambda_{k+1|k}^m(\mathbf{X}), \forall m \in \{1, \dots, M\};$$

**Output:** Reconstructed  $\lambda_{k+1|k}^m(\mathbf{X}), \forall m \in \{1, \dots, M\};$

- 1: **for**  $m \in \{1, \dots, M\}$ ,  $j \in \mathbb{I}_{k|k}^m$ ,  $i \in \mathbb{I}_{k|k}^{m,j}$ ,  $m' \neq m$  **do**
- 2:     **if** (6) and (not recently sent) **then**
- 3:         Compute the handed-over PPP (7);
- 4:         Communicate PPP to BS  $m'$ ;
- 5:         Add (7) to PPP at BS  $m'$  (8);
- 6:     **end if**
- 7: **end for**

After reviewing all the trajectories and incorporating the resulting trajectory PPP intensities into the corresponding predicted trajectory PPP intensities, we update the density at each BS using the relevant measurement set, expressed as

$$f(\mathcal{X}_{k+1}^m | \mathcal{Z}_{1:k+1}^m) = \frac{\tilde{f}(\mathcal{X}_{k+1}^m | \mathcal{Z}_{1:k+1}^m) \ell(\mathcal{Z}_{k+1}^m | \mathcal{X}_{k+1}^m)}{\int \tilde{f}(\mathcal{X}_{k+1}^m | \mathcal{Z}_{1:k}^m) \ell(\mathcal{Z}_{k+1}^m | \mathcal{X}_{k+1}^m) \delta \mathcal{X}_{k+1}^m} \quad (9)$$

with  $\tilde{f}(\mathcal{X}_{k+1}^m | \mathcal{Z}_{1:k+1}^m)$  denoting the density for the  $m$ -th BS, as obtained from Algorithm 1, which involves adding the cor-

<sup>2</sup>We approximate the information as a trajectory PPP rather than directly adding a trajectory Bernoulli to the predicted prior density because the handed-over target has not yet been detected by the  $m'$ -th BS. Since its entry into the  $m'$ -th BS's FoV is based solely on our predictions, which may not materialize. Thus, it is more appropriate for the  $m'$ -th BS to treat this target trajectory as it would with other potentially detectable trajectories that have yet to be observed. Additionally, incorporating the trajectory PPP intensity allows the system to effectively manage repeated information exchanges between the two BSs when the target remains within both FoVs for a duration. The TPMBM filter is more inclined to maintain an existing trajectory rather than initiate a new one from a previously undetected trajectory; therefore, only the trajectory from the initial handover will be retained.

<sup>3</sup>Full details of the management of list of recently handed over target and hyper-parameters to avoid ping-ponging of targets are omitted for space reasons.

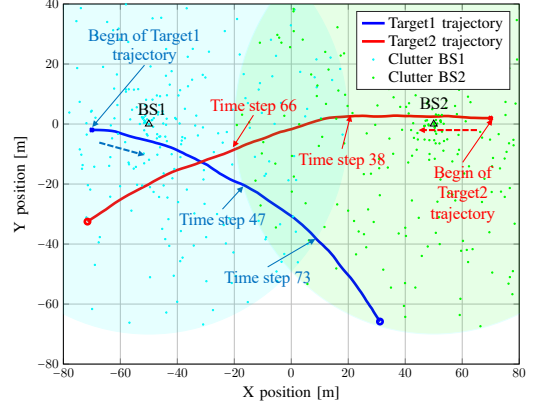


Fig. 2. Simulated scenario with two BSs, and two targets. The clutter for all time step is also shown. Each BS has a limited FoV, while both targets follow a constant velocity movement. Target1 enters BS2's FoV at time step 47 and exits BS1's FoV at time step 73. Target2 enters BS1's FoV at time step 38 and exits BS2's FoV at time step 66.

responding trajectory PPP intensities to its existing trajectory PPP intensity.

## V. NUMERICAL RESULTS

### A. Simulation Environment

We consider a scenario depicted in Fig. 2, where two BSs are positioned at  $[\pm 50 \text{ m}, 0 \text{ m}, 10 \text{ m}]^T$ , respectively, and two targets follow a nearly constant velocity movement over time, with the acceleration noise standard deviation of  $0.05 \text{ m/s}^2$  along both the  $x$  and  $y$  axes, and  $0 \text{ m/s}^2$  along the  $z$  axis. The sampling time is set to 100 ms, and 100 time steps are considered. Target1 starts at  $[-70 \text{ m}, -2 \text{ m}, 1.5 \text{ m}]^T$  with an initial velocity  $[14 \text{ m/s}, 0 \text{ m/s}, 0 \text{ m/s}]^T$ , while the target2 starts at  $[70 \text{ m}, 2 \text{ m}, 1.5 \text{ m}]^T$  with an initial velocity  $[-14 \text{ m/s}, 0 \text{ m/s}, 0 \text{ m/s}]^T$ . The targets are only visible when they are in the FoV of the BSs, set to 70 m. The detection probability is set to 0.9 within the FoV of each BS and 0 outside it, the survival probability is set to 0.99 for both BSs, and the threshold  $\gamma$  is set to 0.5. The measurement noise covariance matrix is fixed to  $\mathbf{R} = \text{diag}[0.1^2 \text{ m}^2, 0.01^2 \text{ rad}^2, 0.01^2 \text{ rad}^2]$ . The clutter intensity  $c(z)$  is set to  $3U_{\text{FOV}}$  for both BSs, with  $U_{\text{FOV}}$  representing a uniform distribution inside the FoV of each BS and 3 representing the expected number of clutter measurements per time step. For the TPMBM implementation, the filters are configured with the following parameters [23], [25]: maximum number of hypotheses is set to 200, the pruning threshold for PPP weights is set at  $10^{-5}$ , the pruning threshold for Bernoulli components is set at  $10^{-5}$ , and a 5-scan implementation is employed. The benchmark algorithm involves independent operation of the BSs, each running a TPMBM filter. The sensing performance is numerically evaluated using the root mean squared (RMS) trajectory error [23] for the trajectory set and the root mean squared error (RMSE) across the given trajectory. We conduct 100 Monte Carlo (MC) simulations for each algorithm, with the final results computed as the average across all independent simulations.

### B. Results and Discussion

Fig. 3 illustrates the RMS trajectory error at BS1 over time for cases with and without the integration of the target

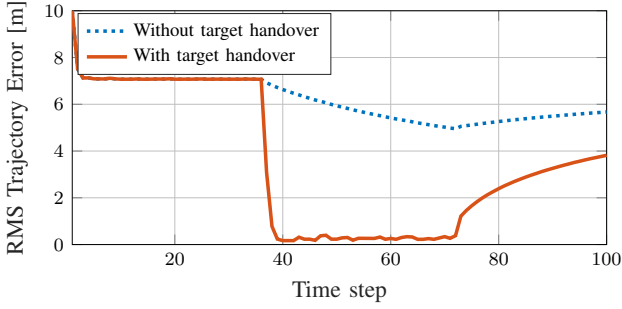


Fig. 3. Comparison of the overall tracking performances of the TPMBM filter with and without the integration of the target handover method at BS1.

handover method. The errors are identical in both scenarios before time step 38, as only target1 is within BS1's FoV, resulting in the same tracking performance. After time step 38, target2 enters BS1's FoV and begins to be tracked, reducing the RMS trajectory error as shown by the decreasing blue dashed line. However, when the target handover scheme is not implemented, BS1 lacks access to target2's earlier trajectory, causing the RMS trajectory error to remain relatively high because part of the trajectory is missed. In contrast, when the target handover scheme is applied, BS1 inherits target2's prior trajectory from BS2 and continues tracking it seamlessly, leading to a significant drop in the red solid line at time step 38. This results in a lower RMS error that persists until time step 73. After time step 73, the errors for both cases increase when target1 leaves BS1's FoV, leading to a loss of tracking.

Fig. 4 displays the RMSE of target2's trajectory at BS1 for both cases. The TPMBM filter effectively tracks target2's full trajectory when the target handover method is used, as BS1 inherits the trajectory information from BS2 at time step 38. Without the target handover scheme, BS1 can only track target2 after it enters its FoV, which is why the red solid line starts at the beginning while the blue dashed line starts at time step 38. Notably, the target handover mechanism provides more accurate estimates immediately after target2 enters BS1's FoV, as the red solid line stays below the blue dashed line between time steps 38 and 47. This is because BS1 inherits a lower-error and lower-covariance trajectory from BS2, allowing it to continue tracking target2 with improved accuracy and lower covariance, compared to starting from an untracked trajectory. However, this gap gradually narrows over time and eventually converges, as both cases receive the same measurements, reducing the impact of the initial error and covariance at time step 38.

Fig. 5 shows the trajectory tracking results from the TPMBM filter at BS2, with the integration of the target handover method. The results show that the TPMBM filter at BS2, when combined with the target handover method, successfully tracks a portion of the target2's trajectory, as indicated by the alignment of the yellow solid line with a section of the red dashed line. Additionally, it tracks the full trajectory of target1, from its origin to the end, indicated by the alignment of the green solid line with the blue dashed lines. Although BS2 cannot track target1 prior to time step 47, since it had not yet entered the BS2's FoV, BS1 hands

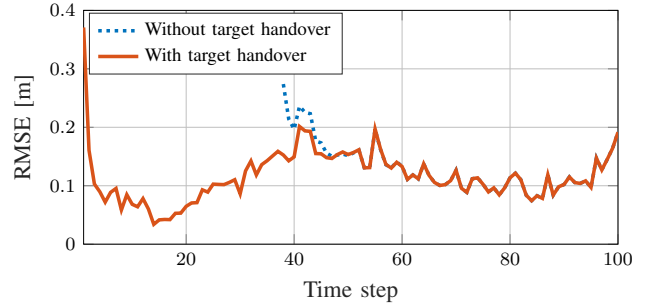


Fig. 4. Comparison of the tracking performances of the TPMBM filter with and without the integration of the target handover method for target2 at BS1.

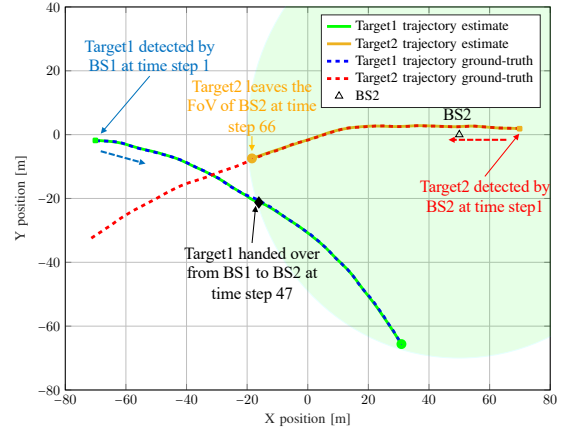


Fig. 5. Tracking results from the TPMBM filter that integrates the target handover method at BS2. Clutter is present but not shown in this visualization.

over all trajectory information about target1 to BS2 at the prediction step of time step 47, just as the target is about to enter the BS2's FoV. BS2 then continues to track target1 based on the inherited trajectory information, resulting in an accurate estimation of target1's full trajectory. Nevertheless, BS2 cannot continue tracking target2 once it leaves its FoV at time step 66. As target2 moved into BS1's FoV, BS2 handed over tracking responsibility to BS1. However, once target2 exits BS2's FoV, the trajectory information is not relayed back to BS2, resulting in a temporary loss of tracking. Notably, during time steps 38 to 66, both BSs track target2 independently, as it remains within the FoVs of BSs.

## VI. CONCLUSIONS

In this paper, we address the target handover problem in DISAC systems by introducing a novel RFS-based target handover algorithm. We provide detailed execution guidelines, including what information to share, when, where, and how it should be transmitted during handover. The proposed target handover mechanism is integrated with the TPMBM filter to address the sensing challenges at each BS. Through simulations, we show that the proposed method efficiently facilitates target handover between BSs as targets enter their FoVs, enabling each BS to track the complete trajectories of targets within its FoV from initial detection until exit. The results also demonstrate that the target handover improves the TPMBM filter's sensing performance, particularly for targets that have recently entered a BS's FoV.

APPENDIX  
BASICS OF TPMBM DENSITY

The structure of the TPMBM RFS resembles that of the Poisson multi-Bernoulli mixture (PMBM) target RFS. In this framework,  $\mathcal{X}$  is viewed as the union of two disjoint trajectory sets  $\mathcal{X}_U$  and  $\mathcal{X}_D$ . Here,  $\mathcal{X}_U$  is the set of undetected trajectories that are hypothesized to exist but never have been detected, i.e., no measurement has been associated with these trajectories. Conversely,  $\mathcal{X}_D$  denotes the set of detected trajectories that exist and have been detected at least once, i.e, associated with at least one measurement before [13], [26]. We model  $\mathcal{X}_U$  as a trajectory PPP, with the density described by

$$f_P(\mathcal{X}_U) = e^{-\int \lambda(\mathbf{X}') d\mathbf{X}'} \prod_{\mathbf{X} \in \mathcal{X}_U} \lambda(\mathbf{X}), \quad (10)$$

where  $\lambda(\cdot)$  represents the trajectory PPP intensity function, defined across the entire trajectory state space. This means that the realizations of the PPP are trajectories with a birth time, a time of the most recent state, and a sequence of states. We model  $\mathcal{X}_D$  as a trajectory multi-Bernoulli mixture (MBM), with the density described by

$$f_{\text{MBM}}(\mathcal{X}_D) = \sum_{j \in \mathbb{I}} w^j \sum_{\mathcal{X}^1 \uplus \dots \uplus \mathcal{X}^n = \mathcal{X}_D} \prod_{i=1}^{|\mathcal{X}_D|} f_B^{j,i}(\mathcal{X}^i), \quad (11)$$

where  $\mathbb{I}$  denotes the index set of all global hypotheses, and  $w^j \geq 0$  represents the weight associated with the  $j$ -th global hypothesis, satisfying  $\sum_{j \in \mathbb{I}} w^j = 1$  [27]. The term  $f_B^{j,i}(\cdot)$  refers to the trajectory Bernoulli density of the  $i$ -th trajectory under the  $j$ -th global hypothesis. Similar to the target Bernoulli, each trajectory Bernoulli follows

$$f_B^{j,i}(\mathcal{X}^i) = \begin{cases} 1 - r^{j,i} & \mathcal{X}^i = \emptyset \\ r^{j,i} f^{j,i}(\mathbf{X}) & \mathcal{X}^i = \{\mathbf{X}\} \\ 0 & \text{otherwise} \end{cases} \quad (12)$$

where  $r^{j,i} \in [0,1]$  denotes the existence probability, and  $f^{j,i}(\cdot)$  represents the trajectory density. For more information on the trajectory PPP and MBM densities, please refer to [13], [26]. The density of  $\mathcal{X}$  can then be calculated using the convolution formula [28, eq. (4.17)] as

$$f(\mathcal{X}) = \sum_{\mathcal{X}_U \uplus \mathcal{X}_D = \mathcal{X}} f_P(\mathcal{X}_U) f_{\text{MBM}}(\mathcal{X}_D), \quad (13)$$

which can also be parameterized by  $\lambda(\mathbf{X})$  and  $\{w^j, \{r^{j,i}, f^{j,i}(\mathbf{X})\}_{i \in \mathbb{I}}\}_{j \in \mathbb{I}}$ , with  $\mathbb{I}^j$  representing the index set of trajectories (i.e., the Bernoulli components) under the  $j$ -th global hypothesis.

REFERENCES

[1] A. Liu, *et al.*, "A survey on fundamental limits of integrated sensing and communication," *IEEE Commun. Surv. Tutor.*, vol. 24, no. 2, pp. 994–1034, 2022.  
[2] F. Liu, *et al.*, "Integrated sensing and communications: Towards dual-functional wireless networks for 6G and beyond," *IEEE JSAC*, 2022.  
[3] E. C. Strinati, *et al.*, "Distributed intelligent integrated sensing and communications: The 6G-DISAC approach," in *Joint European Conference on Networks and Communications & 6G Summit*, 2024, pp. 392–397.

[4] E. C. Strinati, *et al.*, "Towards distributed and intelligent integrated sensing and communications for 6G networks," *arXiv preprint arXiv:2402.11630*, 2024.  
[5] R. Thomä *et al.*, "Distributed ISAC systems – multisensor radio access and coordination," in *European Radar Conference*, 2023, pp. 351–354.  
[6] C. Sturm *et al.*, "Waveform design and signal processing aspects for fusion of wireless communications and radar sensing," *Proceedings of the IEEE*, vol. 99, no. 7, pp. 1236–1259, 2011.  
[7] Y. Ge, *et al.*, "Mmwave mapping and SLAM for 5G and beyond," in *Integrated Sensing and Communications*. Springer, 2023, pp. 445–475.  
[8] A. Yassin, *et al.*, "MOSAIC: Simultaneous localization and environment mapping using mmWave without a-priori knowledge," *IEEE Access*, vol. 6, pp. 68 932–68 947, 2018.  
[9] E. Leitinger, *et al.*, "A belief propagation algorithm for multipath-based SLAM," *IEEE Trans. Wireless Commun.*, vol. 18, no. 12, pp. 5613–5629, Sep. 2019.  
[10] Y. Ge, *et al.*, "A computationally efficient EK-PMBM filter for bistatic mmWave radio SLAM," *IEEE Journal on Selected Areas in Communications*, 2022.  
[11] Y. Ge, *et al.*, "Integrated monostatic and bistatic mmwave sensing," in *IEEE Global Communications Conference*, 2023, pp. 3897–3903.  
[12] L. Svensson *et al.*, "Target tracking based on estimation of sets of trajectories," in *International Conference on Information Fusion*, 2014, pp. 1–8.  
[13] Á. F. García-Fernández, *et al.*, "Multiple target tracking based on sets of trajectories," *IEEE Transactions on Aerospace and Electronic Systems*, vol. 56, no. 3, pp. 1685–1707, 2019.  
[14] J. Kim, *et al.*, "Optimal target assignment with seamless handovers for networked radars," *Sensors*, vol. 19, no. 20, p. 4555, 2019.  
[15] E. T. Yazdi, *et al.*, "Study of target tracking and handover in mobile wireless sensor network," in *The International Conference on Information Networking*, 2014, pp. 120–125.  
[16] Ş. Sönmez, *et al.*, "Handover management for next-generation wireless networks: A brief overview," *IEEE Microwave Theory and Techniques in Wireless Communications*, vol. 1, pp. 35–40, 2020.  
[17] I. Shaya, *et al.*, "Key challenges, drivers and solutions for mobility management in 5G networks: A survey," *IEEE access*, vol. 8, pp. 172 534–172 552, 2020.  
[18] R. W. Heath, *et al.*, "An overview of signal processing techniques for millimeter wave MIMO systems," *IEEE Journal of Selected Topics in Signal Processing*, vol. 10, no. 3, pp. 436–453, 2016.  
[19] Y. Ge, *Single Base Station mmWave Radio Positioning, Mapping, and SLAM*. Chalmers Tekniska Hogskola (Sweden), 2024.  
[20] A. Richter, "Estimation of radio channel parameters: Models and algorithms," Ph.D. dissertation, Ilmenau University of Technology, 2005.  
[21] K. Venugopal, *et al.*, "Channel estimation for hybrid architecture-based wideband millimeter wave systems," *IEEE Journal on Selected Areas in Communications*, vol. 35, no. 9, pp. 1996–2009, 2017.  
[22] F. Jiang, *et al.*, "Beamspace multidimensional ESPRIT approaches for simultaneous localization and communications," *arXiv preprint arXiv:2111.07450*, 2021.  
[23] Á. F. García-Fernández, *et al.*, "Trajectory Poisson multi-Bernoulli filters," *IEEE Transactions on Signal Processing*, vol. 68, pp. 4933–4945, 2020.  
[24] K. Granström, *et al.*, "Poisson multi-Bernoulli mixture trackers: Continuity through random finite sets of trajectories," in *International Conference on Information Fusion*, 2018, pp. 1–5.  
[25] Á. F. García-Fernández, *et al.*, "A metric on the space of finite sets of trajectories for evaluation of multi-target tracking algorithms," *IEEE Transactions on Signal Processing*, vol. 68, pp. 3917–3928, 2020.  
[26] Á. F. García-Fernández, *et al.*, "Poisson multi-Bernoulli mixture filter: Direct derivation and implementation," *IEEE Transactions on Aerospace and Electronic Systems*, vol. 54, no. 4, pp. 1883–1901, 2018.  
[27] J. L. Williams, "Marginal multi-Bernoulli filters: RFS derivation of MHT, JIPDA, and association-based MeMBer," *IEEE Transactions on Aerospace and Electronic Systems*, vol. 51, no. 3, pp. 1664–1687, 2015.  
[28] R. P. Mahler, *Advances in Statistical Multisource-Multitarget Information Fusion*. Artech House, 2014.